Melting process with solid-liquid density change and natural convection in a rectangular cavity

Hoseon Yoo
Department of Mechanical Engineering, Gyeongsang National University, Chinju, Korea

Sung Tack Ro
Department of Mechanical Engineering, Seoul National University, Seoul, Korea

This paper presents a numerical method that simulates the melting process in the presence of solid-liquid density change and natural convection in the melt. The physical model concerned is two-dimensional melting of a phase-change material, initially at its fusion temperature, charged in a rectangular cavity with isothermally heated side walls and an adiabatic bottom wall. The presence of the density change brings no change into the basic form of governing equation, so it is considered through the reformulation of boundary conditions. Difficulties associated with the complex time-dependent melt region, whose shape is also a part of the solutions, are overcome by employing the boundary-fitted coordinate system. Comparison with other works validates the present numerical model and reveals the effects of density change qualitatively. Also, it is confirmed that the present method is preferable to others with natural convection only. Computed results for interesting cases are shown in forms of transient position of the interface, temperature distribution, flow pattern, heat transfer coefficient, and melting fraction as a function of time. Closer examination on melting patterns allows a correlation to be made between the melting fraction and a new independent variable $Ste \cdot Fo \cdot Ra^{1/4}$.

Keywords: phase-change problems; solid-liquid density change; boundary-fitted coordinate system

Introduction

Phase-change heat transfer is important in a wide range of technical processes such as casting, welding, energy storage, development of polar regions, and so on. Therefore, many problems concerning melting or solidification for various geometries and thermal conditions have been investigated. After some earlier experiments[1,2] showed that natural convection in the melt is the primary heat transport mechanism throughout the phase-change process, most numerical studies have concentrated on the coordinate transformation techniques not only to consider its effect in the analysis but to circumvent the computational difficulties due to the irregular-shaped moving boundaries. Works by Saitoh,[3] Hsu et al.,[4] Rieger et al.,[5] and others belong to this class and a comprehensive discussion on them is available elsewhere.[6]

In addition to the natural convection, solid-liquid density change is another important factor that has influence on the phase-change heat transfer. The significance of the phase-change process has been pointed out by some researchers in experimental studies. Sparrow and Broadbent[7] showed that the volume-change-driven motion played a dominant role at an early stage of melting and interacted with natural convective motion as melting proceeded. Also, Ho and Viskanta[8] attributed one of the disagreements between the experimental and numerical results to the omission of the density-change effect in simulation and noted that its effect could not be neglected in the analysis. The first investigation to take this factor into account in the analysis was made by Shamsundar and Sparrow,[9] where only pure conduction was considered as the heat transport mechanism. To make a better prediction on the heat transfer characteristics during melting or solidification, it is obvious that not only natural convection in the melt but the density change should be included in the analysis. However, there have been few attempts to do so. This work, motivated by this fact, investigates a melting process in the presence of both natural convection and the density change.

Since the consideration of the density change brings no additional change into the basic forms of governing equations except that of boundary conditions, a numerical method that was developed for the analysis with natural convection only may be applied by the appropriate reformulations or modifications of boundary conditions. In previous work by the present authors,[10] a coordinate transformation technique using a boundary-fitted coordinate system was proposed and applied to the inward melting with natural convection in a horizontal tube successfully. This method is employed in the present study. The physical model to be treated in this work is a two-dimensional (2-D) melting of a phase-change material (PCM), initially at its fusion temperature, charged in an open-top rectangular cavity with isothermally heated side walls and an adiabatic bottom wall. To allow the free expansion resulting from liquid to solid, the top surface of the PCM is regarded as insulated by air. Although air, of course, is not a perfect insulator, the assumption should be good enough for the purpose of the present problem. In view of the fact that there have been few experiments involving the density change effect

Address reprint requests to Professor Ro at the Department of Mechanical Engineering, Seoul National University, Seoul 151-742, Korea.

Received 23 May 1990; accepted 20 May 1991

reported, the experimental and corresponding numerical results by Ho and Viskanta[8] are a good reference for comparison.

Analysis

Physical model and governing equations

As shown in Figure 1, initially solid-phase PCM at its fusion temperature T_f is charged at a height of H in a rectangular cavity with unit length in depth. From time $t = 0$ side walls are maintained at temperature T_w, which is higher than T_f, while the bottom and top are kept adiabatic. Melting begins along the side walls by heat conduction, but soon the excess volume generated along the solid-liquid interface moves upward to find extra space to fill and forms a free surface over the solid. As the melt layer grows, natural convection begins to develop and accelerates melting. In Figure 1 it can be seen that the level of PCM is slightly higher than the initial height, H.

Since the temperature of the solid is assumed to be that of fusion, the domain to be analyzed becomes the melt region bounded by the interface, bottom wall, side wall, free surface, and line of symmetry. Although the flow in the melt may actually be three-dimensional, a 2-D mathematical model is considered in this work. For simplicity the following assumptions are made:

- the Boussinesq approximation is valid;
- the fluid is Newtonian and incompressible;
- the flow is laminar and 2-D;
- viscous dissipation is neglected.

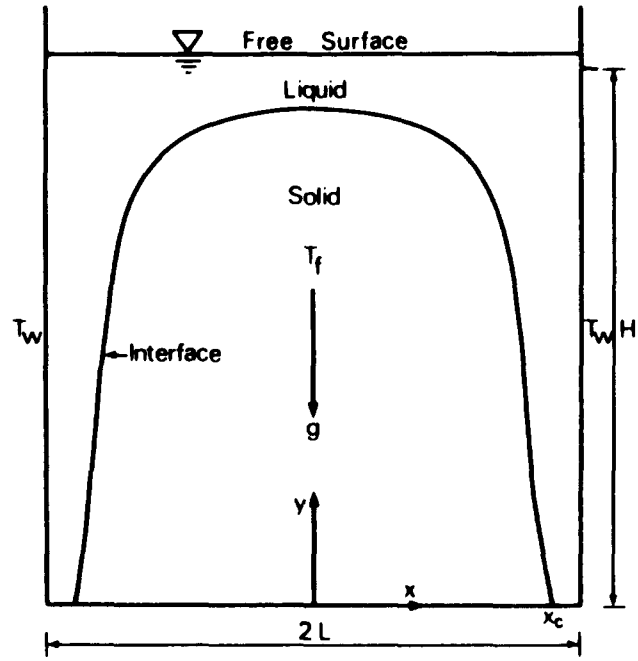

Figure 1 Physical model of present study

Notation

As	Cross-sectional area of unmelted solid
c	Specific heat
f	Arbitrary function
Fo	Fourier number, $\alpha_l t/L^2$
G	Aspect ratio, H/L
g	Gravitational acceleration
H	Initial height of solid
h	Heat transfer coefficient
h_f	Latent heat of fusion
i, j	Unit vector in the direction of x, y
J	Jacobian, $x_\xi y_\eta - x_\eta y_\xi$
k	Thermal conductivity
L	Characteristic length, half width of cavity
n	Normal directional variable
$\boldsymbol{n}$	Outward normal vector
Nu	Nusselt number, $\mathrm{Nu} = hL/k_l$
Pr	Prandtl number, ν_l/α_l
Ra	Rayleigh number, $\beta_T g L^3 (T_w - T_f)/\alpha_l \nu_l$
r_f	Melting fraction
Ste	Stefan number, $c_l(T_w - T_f)/h_f$
T	Temperature
T_f	Fusion temperature
T_w	Wall temperature
t	Time
(u, v)	Transformed velocity component of liquid, $(u, v)^* = (u, v)L/\alpha_l$
V	Velocity vector of liquid
X	Nondimensional interfacial coordinate
(x', y')	Dimensional coordinates
(x, y)	Dimensionless coordinates, $(x, y) = (x', y')/L$
x_c	Position of interface at bottom
Z_i	Dividing points of each boundary
Z_p	Arbitrary points of each interface

Greek symbols

α	$x_\eta^2 + y_\eta^2$
α_l	Thermal diffusivity of liquid
β	$x_\xi x_\eta + y_\xi y_\eta$
β_T	Thermal expansion coefficient of liquid
γ	$x_\xi^2 + y_\xi^2$
Γ_i $(i = 1, 2, 3, 4, 5)$	Boundaries of each region
δ	Thickness of liquid film
θ	Dimensionless temperature, $(T - T_f)/(T_w - T_f)$
μ, ν_l	Viscosity and kinematic viscosity of liquid
(ξ, η)	Transformed coordinates
ρ^*	Liquid-to-solid density ratio, $\rho^* = \rho_l/\rho_s$
τ	Dimensionless time, Ste·Fo
ψ	Dimensionless stream function, $\psi = \psi'/\alpha_l$
ω	Dimensionless vorticity, $\omega = \omega' L^2/\alpha_l$

Subscripts

b	Boundary
f	Fusion
l, s	Liquid, solid
w	Side wall
x, y, ξ, η, τ	Partial derivatives of each quantity

Then, nondimensionalized governing equations in vorticity-stream function formulation on Cartesian coordinates become

$$\mathrm{Ste}\cdot\omega_\tau + \nabla\cdot V\omega = \mathrm{Pr}\,\nabla^2\omega + \mathrm{Ra}\,\mathrm{Pr}\,\theta_x \tag{1}$$

$$-\omega = \nabla^2\psi \tag{2}$$

$$\mathrm{Ste}\cdot\theta_\tau + \nabla\cdot V\theta = \nabla^2\theta \tag{3}$$

where the nondimensionalized quantities are defined in notation.

At the interface between solid and liquid, the energy balance is given by

$$-k_l\left(\frac{\partial T}{\partial x'}\right)_{x'=X'} = h_f\rho_s\frac{\partial X'}{\partial t} \tag{4a}$$

for a one-dimensional (1-D) case. Here x' is used to denote dimensional coordinate and X' indicates interfacial coordinate. The dimensionless form of the equation becomes

$$\frac{\partial\theta}{\partial x} = -\frac{1}{\rho^*}\dot{X} \tag{4b}$$

where ρ^* and $\dot{X}$ denote density ratio of liquid to solid and nondimensional interfacial velocity. Spatial coordinate, x', and interfacial location, X', are nondimensionalized by the half width of the cavity, L to be x and X. Extending Equation 4b to 2-D form and multiplying ourward unit normal vector, $\boldsymbol{n}$,

$$\nabla\theta\cdot\boldsymbol{n} = -\frac{1}{\rho^*}\dot{X}_i\cdot\boldsymbol{n} \tag{4c}$$

can be obtained. In Equation 4c, $\dot{X}_i$ is the nondimensional interfacial velocity. Since the presence of density change makes the interface a kind of volume source, the fluid velocity along the interface is not zero. Mass conservation for the interface gives

$$V_i = -\frac{(1-\rho^*)}{\rho^*}\mathrm{Ste}\,\dot{X}_i \tag{5}$$

Complete descriptions of boundary conditions are treated later.

Coordinate transformations

Regardless of the presence of density change, a coordinate transformation technique is needed to treat the difficulties associated with the complex time-dependent physical domain. In this work, the aforementioned boundary-fitted coordinate system is introduced. Mathematical backgrounds and application of these coordinates were reviewed comprehensively by Thomson et al.[11] Also, detailed numerical techniques for the treatment of the phase-change problems using it can be found elsewhere.[6,10] The advantage of this transformation technique lies in the fact that any set of equations of interest in physical domain may be solved on a rectangular and uniform spaced computational grid that is fixed in time.

The physical domain (x, y) is transformed into computational domain (ξ, η) by

$$\xi_{xx} + \xi_{yy} = R(\xi,\eta) \tag{6a}$$

$$\eta_{xx} + \eta_{yy} = Q(\xi,\eta) \tag{6b}$$

where $R(\xi,\eta)$ and $Q(\xi,\eta)$ are source terms to be chosen. Equations 6a and b are equivalent to

$$\alpha x_{\xi\xi} - 2\beta x_{\xi\eta} + \gamma x_{\eta\eta} = -J^2(Rx_\xi + Qx_\eta) \tag{7a}$$

$$\alpha y_{\xi\xi} - 2\beta y_{\xi\eta} + \gamma y_{\eta\eta} = -J^2(Ry_\xi + Qy_\eta) \tag{7b}$$

where $J = x_\xi y_\eta - x_\eta y_\xi$ denotes Jacobian transformation and α, β, and γ are combinations of x_ξ, x_η, y_ξ, and y_η as given in the notation. In this paper, R and Q are chosen as

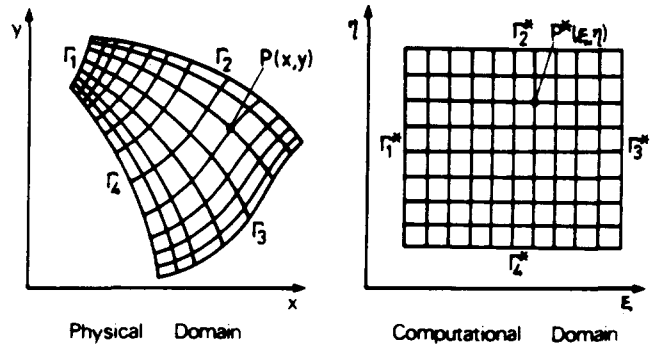

Figure 2 Generation of boundary-fitted coordinate system

$$R = \phi(\xi,\eta)(\xi_x^2 + \xi_y^2) \tag{8a}$$

$$Q = \chi(\xi,\eta)(\eta_x^2 + \eta_y^2) \tag{8b}$$

following the method of Thomas and Middlecoff.[12]

A point $P(x, y)$ at time $\tau = \tau_1$ in the physical domain, which corresponds to $P^*(\xi,\eta)$ in computational domain, as shown in Figure 2, is generated by the numerical solution of the following system of quasi-linear elliptic partial differential equations with Dilichlet conditions along the boundaries:

$$\alpha(x_{\xi\xi} + \phi x_\xi) - 2\beta x_{\xi\eta} + \gamma(x_{\eta\eta} + \chi x_\eta) = 0 \tag{9a}$$

$$\alpha(y_{\xi\xi} + \phi y_\xi) - 2\beta y_{\xi\eta} + \gamma(y_{\eta\eta} + \chi y_\eta) = 0 \tag{9b}$$

$$x = x_b(\xi,\eta) \qquad (\xi,\eta)\in\Gamma_i^* \tag{9c}$$

$$y = y_b(\xi,\eta) \tag{9d}$$

where functions ϕ and χ control the interior grid spacing. The specified forms along the boundaries are[12]

$$\phi = -(x_\xi x_{\xi\xi} + y_\xi y_{\xi\xi})/\gamma \tag{10a}$$

$$x = -(x_\eta x_{\eta\eta} + y_\eta y_{\eta\eta})/\gamma \tag{10b}$$

Then, the values at their interior grid points can be obtained by simple linear interpolation between a pair of boundary curves. For each time step, the same procedure for new boundaries should be repeated. The mapping between physical and computational domains can be written formally as

$$\begin{bmatrix} x \\ y \\ \tau \end{bmatrix} = \begin{bmatrix} x(\xi,\eta,\tau) \\ y(\xi,\eta,\tau) \\ \tau \end{bmatrix} \tag{11}$$

Transformation of original equations into the boundary-fitted coordinate system is no more than mathematical manipulations. Nevertheless, numerical analysis may depend on the form of transformed equations. Therefore, it is important to examine the adequate form for numerical computation. In this work, a geometrically conservative form that is known to preserve the physical meaning of each term of equations under coordinate transformations[11] is taken with modifications. Then, the transformed equations corresponding to Equations 1–3 are cast in the following form:

$$\mathrm{Ste}(J\omega)_\tau + (\bar{u}\omega)_\xi + (\bar{v}\omega)_\eta = \mathrm{Pr}\,\nabla^2\omega + \mathrm{Ra}\,\mathrm{Pr}[(y_n\theta)_\xi - (y_\xi\theta)_\eta] \tag{12}$$

$$-J\omega = \nabla^2\psi \tag{13}$$

$$\mathrm{Ste}(J\theta)_\tau + (\bar{u}\theta)_\xi + (\bar{v}\theta)_\eta = \nabla^2\theta \tag{14}$$

where the differential operator ∇^2 and the transformed velocity

components $(\bar{u}, \bar{v})$ are defined as

$$\nabla^2 f = \left(\frac{\alpha}{J} f_\xi\right)_\xi - \left(\frac{\beta}{J} f_\eta\right)_\xi + \left(\frac{\gamma}{J} f_\eta\right)_\eta - \left(\frac{\beta}{J} f_\xi\right)_\eta \quad (15)$$

$$\bar{u} = y_\eta(u - \text{Ste}\, x_\tau) - x_\eta(v - \text{Ste}\, y_\tau) \quad (16a)$$

$$\bar{v} = x_\xi(v - \text{Ste}\, y_\tau) - y_\xi(u - \text{Ste}\, x_\tau) \quad (16b)$$

And, the transformed relation between stream function and velocity components becomes

$$\psi_\eta = y_\eta u - x_\eta v \quad (17a)$$

$$-\psi_\xi = x_\xi v - y_\xi u \quad (17b)$$

Boundary conditions

The major distinction in the analysis with and without the density change consists in the boundary conditions, one of which was already shown in Equation 4c. Denoting each boundary as Γ_i, $i = 1, 2, 3, 4, 5$ (Figure 3), coordinate lines of the boundary-fitted coordinate system correspond as $\xi = \xi_{min}$ to P_1, $\eta = \eta_{min}$ to Γ_2, $\xi = \xi_{max}$ to Γ_3, and $\eta = \eta_{max}$ to $\Gamma_4 + \Gamma_5$.

For temperature, boundary conditions on the Cartesian coordinate become

$$\nabla\theta \cdot b = 0 \quad \text{at} \quad \Gamma_1, \Gamma_3, \text{ and } \Gamma_5 \quad (18a)$$

$$\theta = 0 \quad \text{at} \quad \Gamma_2 \quad (18b)$$

$$\theta = 1 \quad \text{at} \quad \Gamma_4 \quad (18c)$$

where $\boldsymbol{n}$ is the outward normal vector at each boundary. Transformed forms of Equation 18c are expressed as

$$\alpha\theta_\xi - \beta\theta_\eta = 0 \quad \text{at} \quad \Gamma_1 \text{ and } \Gamma_3 \quad (19a)$$

$$\gamma\theta_\eta - \beta\theta_\xi = 0 \quad \text{at} \quad \Gamma_5 \quad (19b)$$

Since the level of free surface varies due to the density change, boundary conditions for stream function are somewhat complicated. From the definition the following relation is easily obtained:

$$\int_{\Gamma_2} d\psi = -\int_{\Gamma_5} d\psi \quad (20)$$

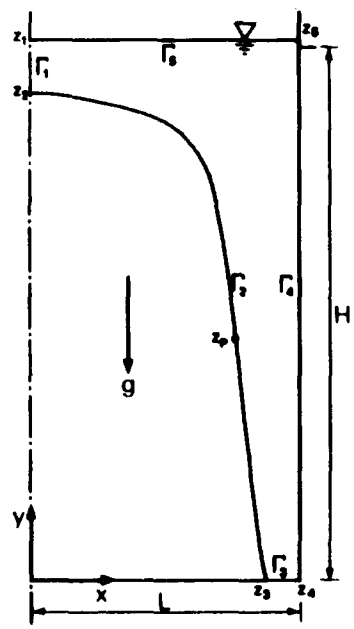

Figure 3 Physical domain of present study

The reference value of ψ, though it is arbitrary, is taken so that ψs at solid walls, Γ_3 and Γ_4 are zero. Then, ψ at Z_p, an arbitrary point on Γ_2, is determined as

$$\psi_{z_p} = \psi_{z_2} - \int_{z_2}^{z_p} V_i \cdot \boldsymbol{n}\, d\Gamma_2 \quad (21a)$$

where V_i is given by Equation 5 and

$$\psi_{z_2} = \int_{z_2}^{z_3} V_i \cdot \boldsymbol{n}\, d\Gamma_2 \quad (21b)$$

Supposing that the free surface is maintained horizontally, the complete set of boundary conditions for stream function except the one already derived can be specified as

$$\psi = \psi_{z_2} \quad \text{at} \quad \Gamma_1 \quad (22a)$$

$$\psi = 0 \quad \text{at} \quad \Gamma_3 \text{ and } \Gamma_4 \quad (22b)$$

$$\psi = (1 - x)\psi_{z_2} \quad \text{at} \quad \Gamma_5 \quad (22c)$$

Transformations of Equations 21a and b result in

$$\psi_{2_p} = -(1 - \rho^*) \cdot \text{Ste} \cdot \int_{\xi_{min}}^{\xi(z_p)} \frac{\gamma}{J} \theta_n\, d\xi + \psi_{z_2} \quad (23a)$$

$$\psi_{z_2} = (1 - \rho^*) \cdot \text{Ste} \cdot \int_{\xi_{min}}^{\xi_{max}} \frac{\gamma}{J} \theta_\eta\, d\xi \quad (23b)$$

where the following were used

$$\begin{bmatrix} x_\tau \\ y_\tau \end{bmatrix}_i = \rho\theta_n \begin{bmatrix} \frac{y_\xi}{J} \\ -\frac{x_\xi}{J} \end{bmatrix}_i \quad (24a)$$

$$d\Gamma_2 = \gamma^{1/2}\, d\xi \quad (24b)$$

$$\boldsymbol{n} = \frac{1}{\gamma^{1/2}} \begin{bmatrix} -y_\xi \\ x_\xi \end{bmatrix} \quad (24c)$$

Vorticity at the solid wall that affects the flow field directly cannot be specified a priori but is obtained as a part of the solution. There have been a number of methods[13] to specify the vorticity at the solid wall, but no absolute measure of selection exists. It depends on the problems concerned. A modified form of the method by Gosman et al.[14] has proved superior in convergence for this problem by numerical analysis. Vorticities at the line of symmetry and the free surface can be readily determined by definition. The final form of the vorticities at the boundaries adopted in this work are

$$\omega = 0 \quad \text{at} \quad \Gamma_1 \text{ and } \Gamma_5 \quad (25a)$$

$$\omega = -2\left(\frac{\gamma}{J^2}\right)(\psi_{nw} - \psi_{sw} - u_t) \quad \text{at} \quad \Gamma_2 \quad (25b)$$

$$\omega = -2\left(\frac{\gamma}{J^2}\right)(\psi_{nw} - \psi_{sw}) \quad \text{at} \quad \Gamma_3 \quad (25c)$$

$$\omega = -2\left(\frac{\gamma}{J^2}\right)(\psi_{nw} - \psi_{sw}) \quad \text{at} \quad \Gamma_4 \quad (25d)$$

where u_t, ψ_{nw}, and ψ_{sw} denote tangential velocity component of fluid at the interface, stream functions at a unit distance normal to the wall and at the wall, respectively.

The above vorticity conditions at the walls can be derived as follows. When we assume that solid boundary is fixed and transformed coordinates are orthogonal near solid walls and the tangential gradients are much smaller than normal ones at

solid walls, vorticity Equation 12 can be approximated as

$$\left[\bar{v}\omega - \mathrm{Pr}\left(\frac{\gamma}{J}\right)\omega_n + \mathrm{Ra}\,\mathrm{Pr}\, y_\xi \theta\right]_n = 0 \tag{26}$$

where n denotes a normal directional variable. Integrating Equation 26 for n and neglecting tangential velocity $\bar{v}$, ω_n is obtained. Another integration gives

$$\omega = \omega_n \cdot \boldsymbol{n} + \omega_{sw} \tag{27}$$

where ω_{sw} denotes vorticity at the solid wall. Equation 13, vorticity-stream function relation, can be integrated similarly with the aid of Equation 27 to give

$$\Psi - \Psi_{sw} = -\left[(\omega_n)_{sw}\frac{n^3}{6} + \omega_{sw}\frac{n^2}{2}\right]\left[\frac{J^2}{\gamma}\right] \tag{28}$$

When it is assumed that the vorticity is uniform near solid walls, the following relation is obtained:

$$\omega_{sw} = -2\left[\frac{\gamma}{J^2}\right][\Psi_{nw} - \Psi_{sw}] \tag{29}$$

where Ψ_{nw} denotes stream function at unit length, $n = 1$, from solid wall. This applies for solid boundaries Γ_3 and Γ_4, and a similar relation can be obtained for the interface Γ_2.

Initial conditions

Initially, the whole system is in the solid phase so that in physical domain the region of liquid phase cannot be defined. However, it is possible to start numerical computations by assuming melting takes place along the heating wall to the extent of sufficiently small gap width. The analytical solution for 1-D semi-infinite solid yields the position of the interface from the wall and temperature distribution.

That is,

$$X = 2K(\tau_0/\mathrm{Ste})^{1/2} \tag{30a}$$

$$\theta = 1 - \frac{\mathrm{erf}\left[(\mathrm{Ste}/\tau_0)^{1/2}\cdot\frac{x}{2}\right]}{\mathrm{erf}(K)} \tag{30b}$$

where K is the solution of

$$K\cdot\exp(K^2)\cdot\mathrm{erf}(K) = \rho^*\cdot\frac{\mathrm{Ste}}{\pi^{1/2}} \tag{30c}$$

Here τ_0 represents a sufficiently short time during which conduction heat transfer can be assumed.

Also, it is assumed that the excess volume generated by the density change in this gap moves upward and forms a thin liquid layer with the free surface. Then, initial physical domain for numerical computation consists of a small liquid gap along the heating wall and a connected thin liquid layer over the solid. The upper layer is so thin that the initial temperature distribution over it can hardly have influence on the later behaviors.

Numerical procedure

Terms of the transformed governing equations are similar in form and physical meaning to those of originals except the cross-differential ones. So, it is possible that a numerical method that was originally developed for orthogonal coordinates can be applied to this case if the cross-differential terms can be handled reasonably. Shyy et al.[15] have explored this fact for the analysis of a steady-state laminar flow field in irregular geometry. Also, it has been proved to be successful for the melting problem by the present authors.[10] Transformed governing equations and corresponding boundary conditions are discretized using the control-volume formulation proposed by Patankar.[16] In the actual computation, the cross-differential terms have been treated as source terms.

To avoid a large memory and excess computing time, a sequential computation procedure is employed, i.e., for one time step computations are performed in the following order:

(1) computation of (x_τ, y_τ) from information at the previous time step;
(2) generation of grid system and computation of the grid velocity;
(3) solution of equations for energy, vorticity, and stream function in turn.

If the solution satisfies a prescribed convergence criterion, computations move to the next time step, otherwise step 3 is repeated.

The grid system is structured by (33, 15) nodal points in (ξ, η) directions. Since the nodes on the boundaries concentrate or disperse as the curvature of boundary varies, the rezoning process is necessary to maintain the properly structured grid system. It was accomplished by the cubic spline fitting of the interface and redistribution of nodes on the boundaries at each time step. Time increment $\Delta\tau$ is taken as 10^{-5} considering the numerical instabilities.

Result and discussion

Definition of parameters

Heat transfer during melting may be characterized by the heat transfer coefficient at the heating wall. The local wall Nusselt number, Nu_w, a nondimensionalized form of the local heat transfer coefficient, is defined and expressed on the transformed coordinates as

$$\mathrm{Nu}_w = h_w L/k_l = \left(\frac{\partial\theta}{\partial n}\right)_w = \left(\frac{\gamma^{1/2}}{J}\theta_\eta\right)_w \tag{31}$$

The average wall Nusselt number, $\overline{\mathrm{Nu}}_w$, is defined as an average of Nusselt numbers along the boundary of the heating surface contacting the PCM. The contacting area or length increases due to volume expansion of PCM as the melting fraction increases with time. The average wall Nusselt number as a function of time can be readily calculated from

$$\overline{\mathrm{Nu}}_w = \frac{1}{l}\int \mathrm{Nu}_w\, dx = \frac{\int\left(\frac{\gamma}{J}\theta_\eta\right)_w d\xi}{\int(\gamma^{1/2})_w\, d\xi} \tag{32}$$

where l represents the total length of walls contacting PCM.

Melting fraction, r_f, is defined as the ratio of mass in liquid phase to total mass. The expression for r_f becomes

$$r_f = \frac{1}{\rho_s HL}\int \rho_i\, dx\, dy = \frac{\rho^*}{G}\int J\, d\xi\, d\eta \tag{33}$$

Here the integration covers the region in liquid phase and G denotes aspect ratio of H/L. In present computation, $G = 2$ is taken.

Rayleigh number is used in the analysis. One half width of system L, which is invariant, is used as the characteristic length for nondimensionalization.

Effect of density change

Computations are performed for the cases: one without density change and another with a density ratio of $\rho^* = 0.95$. Com-

parison is made only with the work by Ho and Viskanta.[8] They reported experimental data and numerical results obtained using the Landau transformation technique without consideration of the density change. One representative case is chosen to compare. Throughout the present study, the ratio of liquid to solid density of PCM is fixed at $\rho^* = 1$ and $\rho^* = 0.95$. The latter can be applied to n-octadecane ($\rho_s = 814$, $\rho_l = 768$ kg/m^3).

The melting fractions are illustrated in Figure 4 as a function of dimensionless time. The figure shows comparison of the melting fractions at Ra = 0.788×10^7 and Ste = 0.063. Two solid lines indicate the present calculation of the fractions for density ratio $\rho^* = 1$ (no density change) and $\rho^* = 0.95$. The numerical result of Ho and Viskanta[8] is represented by a dotted line, and the symbols are for experimental data by the same authors. Analytic solution for melting by pure conduction only is also presented as a reference.

At the initial stage the calculated melting fractions for $\rho^* = 1$ agrees well with those of Ho and Viskanta[8] and pure conduction, but a discrepancy appears as time elapses. As time increases, the calculated results of Ho and Viskanta fall well below the present calculations for $\rho^* = 1$ and $\rho^* = 0.95$. This fact was already indicated in the scaling theory of melting by Jany and Bejan.[17] At the beginning of melting, the density change by volume expansion generates an extra movement of liquid to accelerate melting. The effect of density change diminishes with time although the amount of excess melting fraction remains. Figure 4 is redrawn to exclude the conduction term. Normalized melting fraction is defined as melting fraction normalized by the fraction due to conduction only and is given in Figure 5. The calculated result by Ho and Viskanta[8] is also presented for comparison. It is believed that the abrupt increase in $\rho^* = 0.95$ at the very early stage is due to the volume-change-driven motion. As the melt gap grows, the relative contribution by the excess volume decreases.

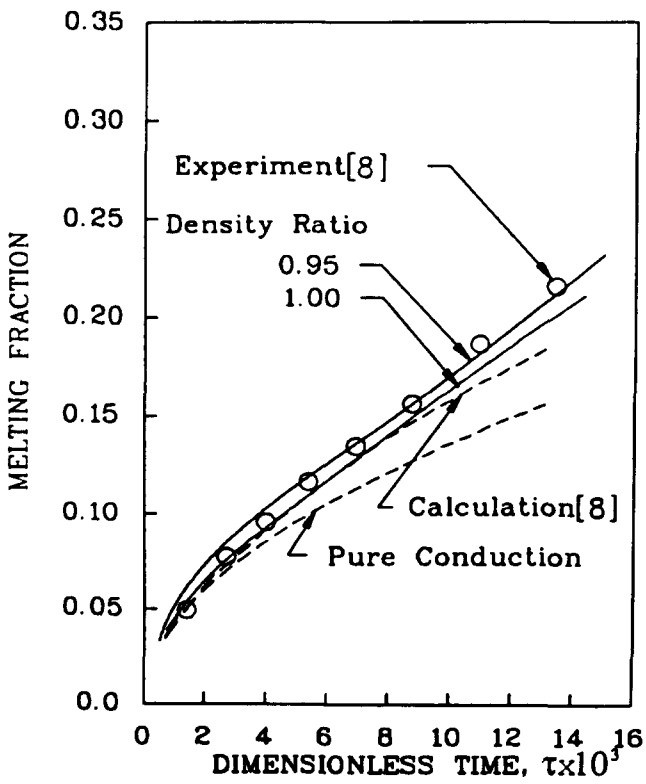

Figure 4 Comparison of melting fractions for Ra = 0.788×10^7 and Ste = 0.063

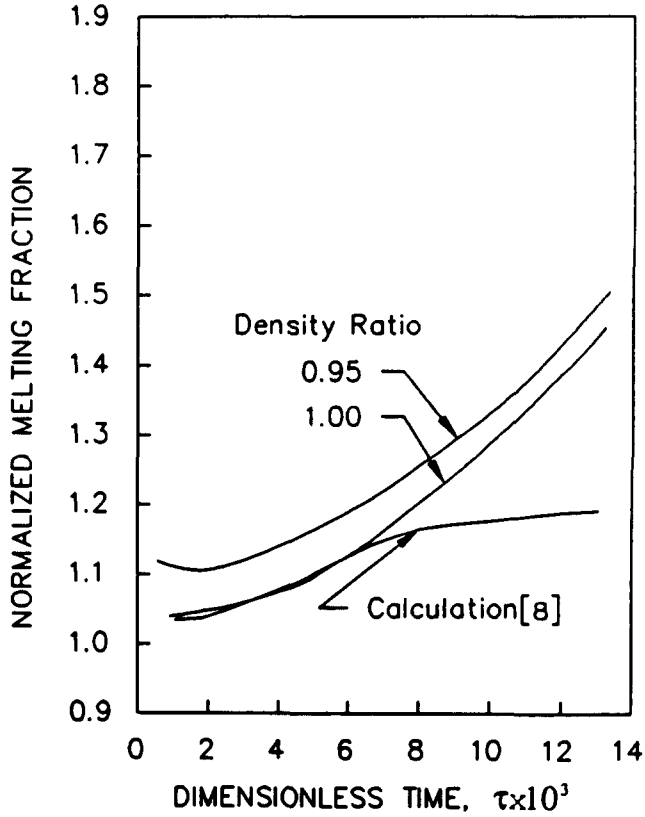

Figure 5 Normalized melting fractions with and without density change

Figure 6 shows the average wall Nusselt numbers for various cases including the data from Ho and Viskanta[8] and the result for pure conduction. One of the reasons for the disagreement seems to be the subcooling effect in the experiment. According to the investigation by Kemink and Sparrow,[18] timewise variation of the heat transfer coefficient with initial subcooling of the solid in the melting process is expressed as lower in absolute value and rightward shifted in time compared with that without subcooling. The rightward shift may arise due to the heat supply condition at the heating wall. The effect of the density change on Nusselt number is similar to that of the melting fraction in Figure 4.

Influences of various parameters

Since the numerical computations were very time consuming in spite of a relatively large time increment and less severe convergence criteria, simulations to investigate the influences of dimensionless parameters on the melting processes are performed for a limited number of cases. Computed results for Pr = 5 and 50 were compared first and they coincided exactly with each other. This fact meets with the study by Sparrow et al.[18] where Pr = 7 and 70 were treated.

Since the experiments for various geometries have provided conclusive evidence that natural convection heat transfer controls the phase-change processes, the role of the Rayleigh number might be important. To reconfirm this fact and get the quantitative informations, three cases, Ra = 0.788×10^7, 1.57×10^7, and 2.5×10^7, are compared. As expected, a high Rayleigh number accelerates the development of natural convection decisively. In Figure 7, the local minimum of the average Nusselt number at the heating wall, which is known as an indication of transition from heat conduction to natural convection dominant regime[19], appears in advance as the Rayleigh

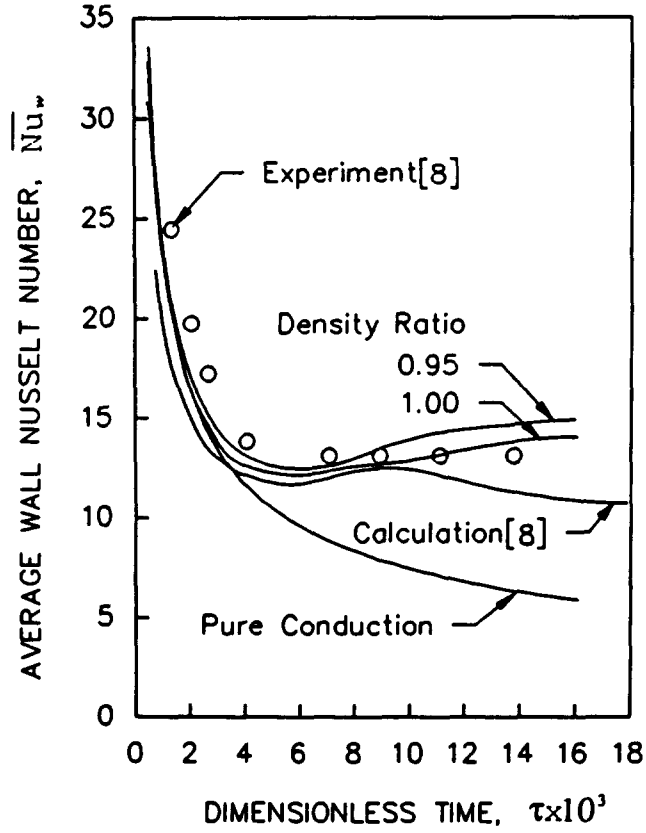

Figure 6 Comparison of average wall Nusselt number for Ra = 0.788 × 10^7 and Ste = 0.063

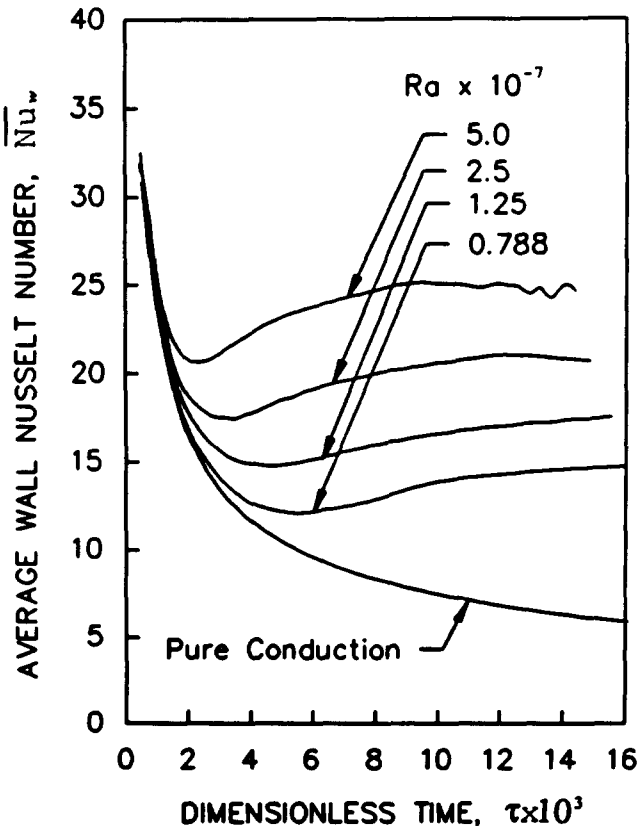

Figure 7 Effect of Rayleigh number on average Nusselt number

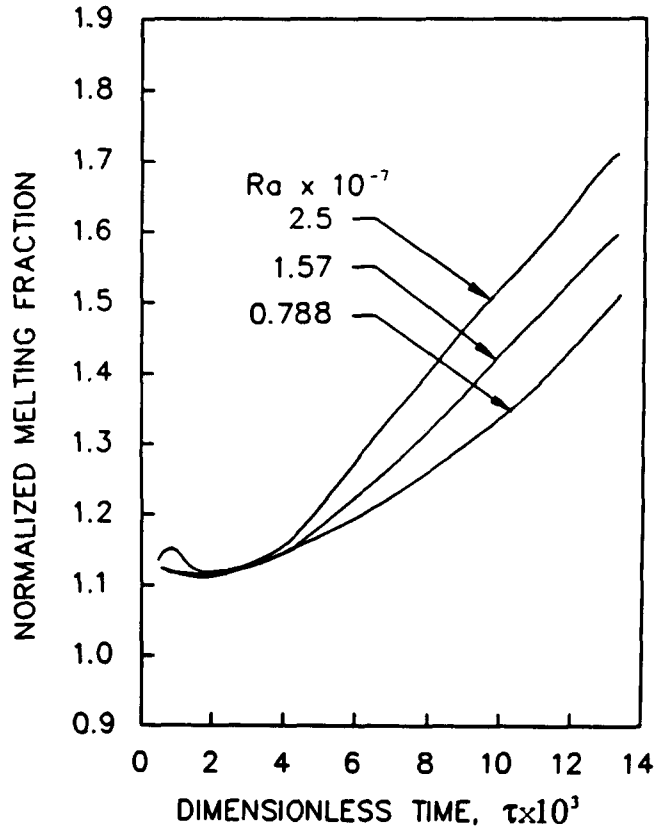

Figure 8 Normalized melting fraction for various Rayleigh numbers

number increases. Although the absolute values of each curve are different, the timewise variation trend is similar, i.e., following the sharp decrease at early times and the local minimum, the Nusselt number increases gradually toward a quasi-steady state. This fact represents that increase of Rayleigh number that does not bring drastic changes to the melting process but advances the onset time of natural convection and intensifies it more quickly. The uppermost curve oscillates after the time $\tau = 11 \times 10^{-3}$. If the secondary flows took place in the corresponding flow field, this phenomenon can be regarded as the transition of the flow regime from a quasi-steady to an unstable state.[20] In this case, however, it seems to be induced by numerical instabilities because there were no secondary flows. Probably, a relatively high velocity by a large Rayleigh number and coarse grid system compared with wide melt region causes the numerical computation to be unstable as the melting proceeds. However, it is necessary to study further to clarify it.

Figure 8 shows normalized melting fraction as a function of time for three different Rayleigh numbers in the case of $\rho^* = 0.95$. No further explanation may be needed.

Flow pattern and temperature distribution

Flow patterns and temperature distributions for Ra = 2.5 × 10^7 are presented in Figures 9 and 10, respectively. In Figure 9, it is worth noting that at an early time the maximum of stream function is located near the top of the narrow melt gap along the heating wall. As the melting continues, the convective recirculating flow is intensified while its maxima move toward the center of the melt layer. The corresponding temperature profiles (Figure 10) also show this pattern, i.e., parallel isotherms are distorted from top to middle of the vertical layer, making a larger gradient in the x-direction.

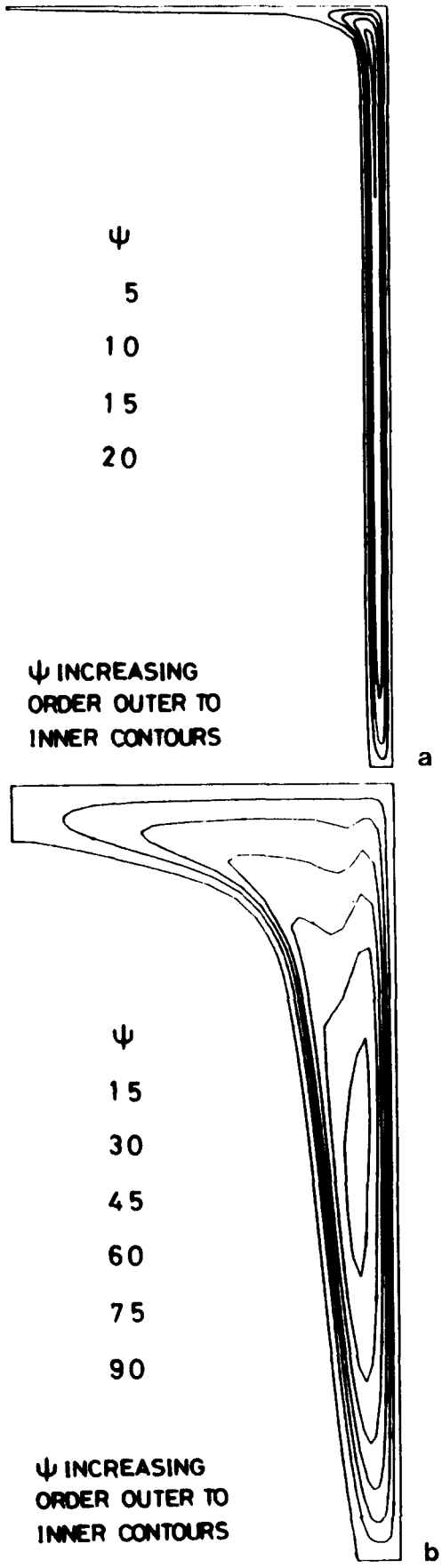

Figure 9 Timewise variation of flow patterns for Ra = 2.5×10^7 and $\rho^* = 0.95$ (*a*) at $\tau = 2.5 \times 10^{-3}$ and (*b*) at $\tau = 14.5 \times 10^{-3}$

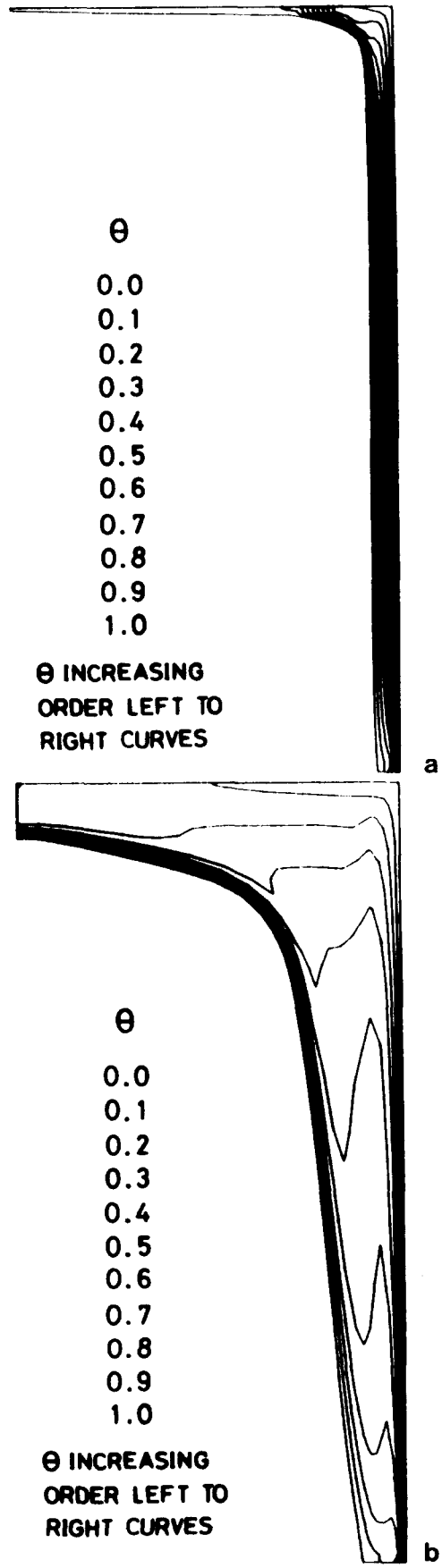

Figure 10 Timewise variation of temperature distributions for Ra = 2.5×10^7 and $\rho^* = 0.95$ (*a*) at $\tau = 2.5 \times 10^{-3}$ and (*b*) at $\tau = 14.5 \times 10^{-3}$

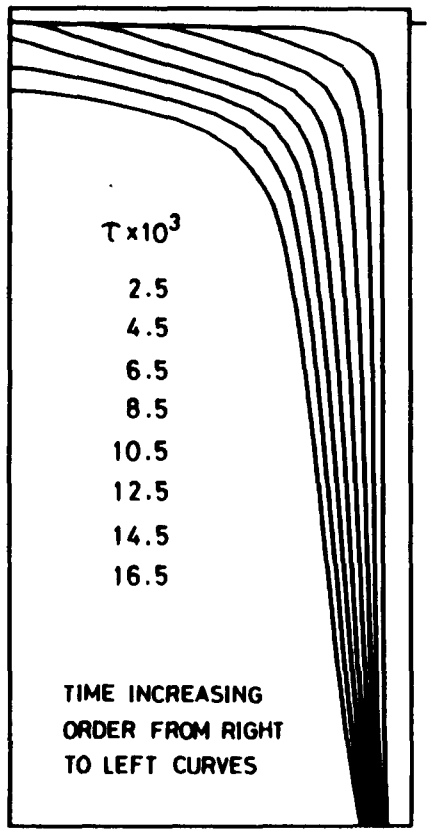

Figure 11. Transient solid-liquid interface position for Ra = 2.5 × 10^7 and $\rho^* = 0.95$

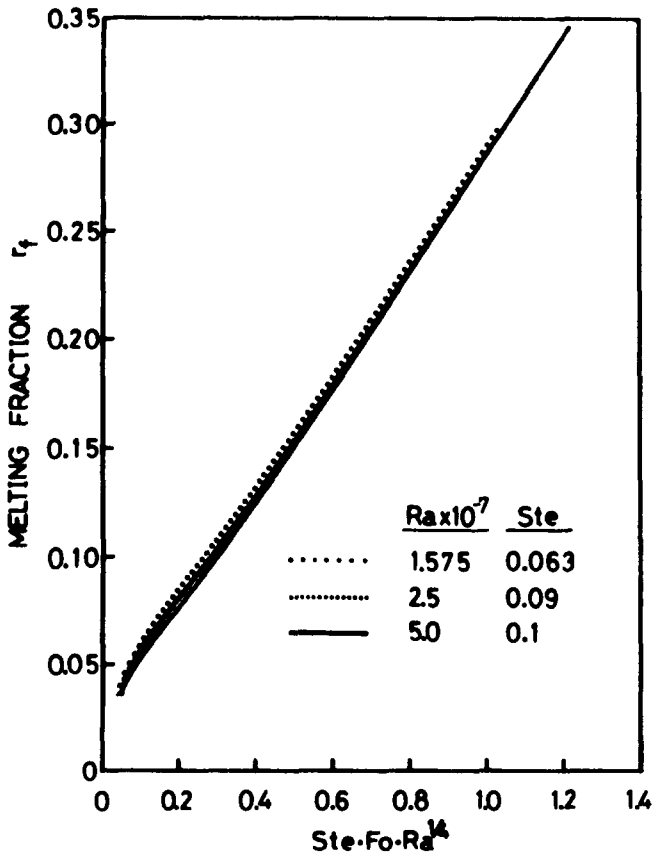

Figure 12 Correlation for melting fraction as a function of Ste·Fo·$Ra^{1/4}$

Figure 11, timewise change of the interface shape, shows the nature of the melting pattern. At the early stage of melting, a thin melt layer along the free surface becomes the passage for supplying heat to the flat top of the solid, which impels this zone to melt and thickens the upper layer. This is consistent with the predicted flow pattern and temperature distribution, where a temperature gradient normal to the interface is developed gradually along the upper part of the solid. In the result, a remarkable melting takes place at this part. Here, the primary mechanism for heat transport is, of course, the natural convection.

Correlation of the melting fraction

One of the most significant results of research on the melting process is the melting fraction. If the melting fraction can be expressed as a function of a new independent variable regardless of changes in the parameters, it will be very convenient for practical purposes. As discussed, the influence of Rayleigh number was predominant over that of the others. Moreover, a similar trend of the melting fraction was preserved when Rayleigh number changed. So, it was deduced that the new independent variable should be expressed in terms of Rayleigh number. It was found to be Ste·Fo·$Ra^{1/4}$. Figure 12 shows the correlation of the predicted melting fraction with respect to the new variable. Curves coincide quite well and the correlation functional form is almost linear.

Conclusion

A numerical study on two-dimensional melting of a PCM in a rectangular cavity with isothermally heated vertical side walls has been carried out. The solid-liquid density change that accompanies phase-change process as well as natural convection in the melt was considered in the analysis. To overcome the difficulties associated with the time-dependent irregular domain, a coordinate transformation technique using the boundary-fitted coordinate system was employed. Based on the comparisons of computed results with others and some simulations to investigate the influences of parameters, the following are clarified:

- The predictions on the melting behaviors made by the present method are physically meaningful and show better agreement with the experimental results than those of the others. Therefore, the density-change effect should be considered in the analysis of the phase-change process to make better predictions.
- The effect of the density change appears clearly at the early stage of the process and acts as a kind of supplementary means to convey heat from the heating wall to the solid-liquid interface combined with natural convection at later times.
- Rayleigh number affects the process most significantly. A large Rayleigh number advances onset time of natural convection and magnifies its intensity, so that the melting is accelerated.
- For the practical use, a correlation of the melting fraction is obtained as a function of Ste·Fo·$Ra^{1/4}$.

Acknowledgment

The work was supported by the Korea Science and Engineering Foundation through Seoul National University. The authors thank Dr. Y. P. Lee and Mr. J. S. Suh for their effort to revise the manuscript.

References

1 Sparrow, E. M., Schmidt, R. R., and Ramsey, J. W. Experiment on the role of natural convection in the melting of solids. *J. Heat Transfer*, 1978, **100**, 11–16

2 Bathelt, A. G., Viskanta, R., and Leidenfrost, W. An experimental investigation of natural convection in the melt region around a heated horizontal cylinder. *J. Fluid Mech.*, 1979, **90**, part 2, 227–239

3 Saitoh, T. Numerical method for multi-dimensional freezing problems in arbitrary domains. *J. Heat Transfer*, 1978, **100**, 294–299

4 Hsu, C. F., Sparrow, E. M., and Patankar, S. V. Numerical solution of moving boundary problems by boundary immobilization and a control-volume-based finite-difference scheme. *Int. J. Heat Mass Transfer*, 1981, **24**, 1335–1343

5 Rieger, H., Projahn, U., and Beer, H. Analysis of the heat transport mechanisms during melting around a horizontal circular cylinder. *Int. J. Heat Mass Transfer*, 1982, **25**, 137–147

6 Yoo, H. Numerical analysis of the phase change process with solid-liquid density change and natural convection. PhD Thesis, Department of Mechanical Engineering, Seoul National University, Seoul, Korea, 1986

7 Sparrow, E. M., and Broadbent, J. A. Inward melting in a vertical tube which allows free expansion of the phase-change medium. *J. Heat Transfer*, 1982, **104**, 309–315

8 Ho, C. J., and Viskanta, R. Heat transfer during melting from an isothermal vertical wall. *J. Heat Transfer*, 1984, **106**, 12–19

9 Shamsundar, N., and Sparrow, E. M. Effect of density change on multidimensional conduction phase change. *J. Heat Transfer*, 1976, **98**, 550–557

10 Yoo, H., and Ro, S. T. Numerical analysis of the phase change processes by coordinate transformations. *Trans. Korean Soc. Mech. Eng.*, 1986, **10**, 585–592

11 Thomson, J. F., Warsi, Z. U. A., and Mastin, C. W. Boundary-fitted coordinate systems for numerical solution of partial differential equations—a review. *J. Comput. Phys.*, 1982, **47**, 1–108

12 Thomas, P. D., and Middlecoff, J. F. Direct control of the grid point distribution in meshes generated by elliptic equations. *AIAA J.*, 1980, **18**, 652–656

13 Roache, P. J. *Computational Fluid Dynamics*. Hermosa Publishers, Albuquerque, 1972

14 Gosman, A. D., Pun, W. M., Runchal, A. K., Spalding, D. B., and Wolfstein, M. *Heat and Mass Transfer in Recirculating Flow*. Academic Press, San Diego, 1973

15 Shyy, W., Tong, S. S., and Correa, S. M. Numerical recirculating flow calculation using a body-fitted coordinate system. *Numerical Heat Transfer*, 1985, **8**, 99–113

16 Patankar, S. V. *Numerical Heat Transfer and Fluid Flow*. Hemisphere Publishing Corporation, 1980

17 Jany, P., and Bejan, A. Scaling theory of melting with natural convection in an enclosure. *Int. J. Heat Mass Transfer*, 1988, **31**, 1221–1235

18 Kemink, R. G., and Sparrow, E. M. Heat transfer coefficients for melting about a vertical cylinder with or without subcooling and for open or closed containment. *Int. J. Heat Mass Transfer*, 1981, **24**, 1699–1710

19 Sparrow, E. M., Patankar, S. V., and Ramadhyani, S. Analysis of melting in the presence of natural convection in the melt region. *J. Heat Transfer*, 1977, **99**, 520–526

20 Rieger, H., Projahn, U., Bareiss, M., and Beer, H. Heat transfer during melting inside a horizontal tube. *J. Heat Transfer*, 1983, **105**, 226–234